ON THE DIFFERENCE BETWEEN ISOTHERMAL AND NON-ISOTHERMAL REDUCTION TESTS: A COMPARISON BETWEEN COREM R180 AND ISO DR90*

Laforest, Guylaine[1]
Dubé, Mathieu[2]
Lacroix, Olivier[3]

Abstract
The reduction behavior of iron ore pellets in gas-based DR shaft processes has been studied at COREM since the late 80s. At that time, a new DR characterization test called COREM R180 was developped in collaboration with ArcelorMittal Mines Canada (former Quebec Cartier Mining) and ArcelorMittal Long Products Canada (former ISPAT Sidbec Inc.). This paper describes COREM's approach to improve its understanding of the relations between iron ore pellet microstructure and pellet quality. The differences between the DR90 and the R180 tests are discussed. The evolution of the microstructure during reduction of both tests is also described. The reduction steps during the two tests are put forward as an important factor impacting the microstructural changes as well as the test results.

Keywords: Iron ore pellets, optical microscopy, direct reduction, DR90, COREM R180, metallisation.

[1] *Eng., Ph. D., Researcher, Agglomeration and Thermal Processing, COREM, Quebec, City, Quebec, Canada.*
[2] *Eng., Researcher and Program Leader, Agglomeration and Thermal Processing, COREM, Quebec, City, Quebec, Canada.*
[3] *Eng., M.Sc., Researcher, Agglomeration and Thermal Processing, COREM, Quebec, City, Quebec, Canada.*

** Technical contribution to the 49º Seminário de Redução de Minério de Ferro e Matérias-Primas e 7º Simpósio Brasileiro de Aglomeração de Minério de Ferro, part of the ABM Week 2019, October 1st-3rd, 2019, São Paulo, SP, Brazil.*

1. INTRODUCTION

COREM is the largest research center in Canada totally devoted to mineral processing R&D. One of the research axes in iron ore pelletizing is fired pellet quality. COREM's focus is on improving the understanding of the links between pellets' physical and metallurgical properties, their microstructure, the pelletizing process variables and the reduction behavior in industrial processes.

This paper makes a comparison between two DR characterization tests, namely DR90 and COREM R180.

2. METHODOLOGY

2.1 Reduction

COREM R180 uses the same set-up as that of ISO DR90 reducibility and metallization test for DR feedstock (ISO 11258). The sample holder is a vertical cylinder (75 mm inner diameter) having the form of a torch. The bottom of the sample holder is fixed to a steel plate supported by four legs. A larger vertical cylinder covers the sample holder and seals the gas chamber at the steel plate level. The assembly in its entirety is placed on a digital balance connected to a computer for data acquisition and computation. A vertical tube furnace is installed over the sample holder assembly. This furnace is electrically heated and can reach a maximum temperature of 1200 °C. The furnace temperature is controlled and recorded by a Foxboro DCS (Distributed Control System). The sample's temperature is measured with a type K thermocouple and recorded by the same DCS. The reduction gas composition and flow rates are controlled by electronic mass flow meters/controllers connected to the Foxboro DCS. The gas is introduced at the bottom of the steel plate and passes through the gas chamber where it is preheated. The gas penetrates in the sample by the top and comes out at the bottom of the sample holder, under the steel plate. The outlet gas is burned before being released to the atmosphere.

The test conditions for the R180 and ISO DR90 are summarized in Table 1. Procedure and reproducibility of the R180 test were fully detailed in previous publication [2].

Table 1. Test conditions for R180 compared to ISO DR90

Test	R_{180} (COREM)			DR_{90} (ISO 11258)
Reactor	Vertical cylinder with weighting device 75 mm inside diameter			Vertical cylinder with weighting device 75 mm inside diameter
Sample Weight	500 ± 0,1 g			500 ± 0,1 g
Pellet size	100 %, -12,5 + 10 mm			50 %, -12.5 + 10 mm 50 %, -16 + 12,5 mm
Temperature	400 to 850 °C ± 5 °C			800 °C ± 5 °C
Reduction time	180 minutes			90 minutes
Reduction gas	Mix 1	Mix 2	Mix 3	Mix 1
% CO	5,5	14.0	26.0	30.0
% CO2	28,5	20.0	8.0	15.0
% H2	61,0	61.0	61.0	45.0
% N2	5.0	5.0	5.0	10.0
Total flow (l/min)	30.0	30.0	30.0	50.0
Results	% reduction after 180 min.			% reduction after 90 min. % metallization calc.

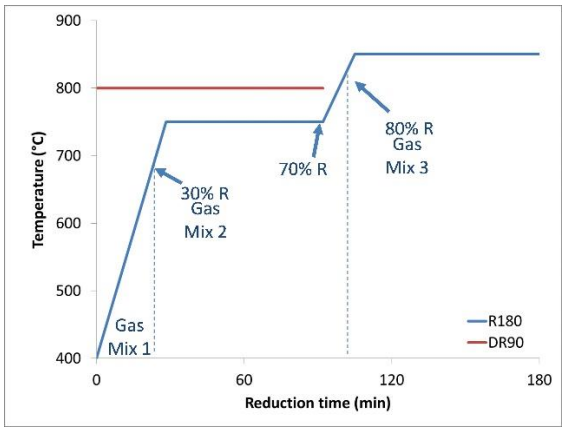

Modified DR90 and R180 tests were also performed. Modified tests are described in Table 2. Modified tests were performed on 100%-12.5+10.0 mm pellets.

Table 2. Description of modified tests

Test ID	Description
Modification 1	DR90 until 70% R and then R180 till 180 min
Modification 2	DR90 until 30% R and then R180 till 180 min
Modification 3	R180 until 30% R and then DR90 till 180 min
Modification 4	R180 until 10% R and then DR90 till 180 min

2.2 Microstructure analysis

The microstructure was analyzed with an optical microscope coupled to a commercial and in-house image analysis software.

The system scans four polished sections of five half-pellets in sequence with a white color check using a grain of metallic iron for quality control between the acquisitions of each section. Each picture is classified in different concentric zones from the core to the shell of the pellet. Each mineral phase has its specific color range and can be discriminated from the other mineral phases.

After some spatial and spectral filtering, the amount, in vol%, of metallic iron, iron oxide and porosity can be determined for reduced pellets. These results are then compiled and averaged over 30 pellets of the same sample. Overall, more than 45000 images are analyzed per sample. Further description as well as the precision of the measurement and application to fired pellets can be found in a previous paper [1].

As a post processing measurement on the different images, the specific surface areas and mean linear size (mls) of the mineral phases were calculated. The specific surface area S_v (cm^2/cm^3) [1] is related to the number of intersection points P, (cm^{-1}) between a given phase and a test line in Equation 1:

$$S_v = 2P_L \quad (1)$$

The mean linear size (µm) is defined by Equation 2 [1] where V_V is the volumetric fraction of a given phase:

$$\text{mls} = 2V_V / (S_V/10\,000) \quad (2)$$

The specific surface and the mls of each phase can be calculated. Furthermore, the specific surface can also be broken down in such a way that it is possible to characterize the contact between the phases.

Table **3** summarizes the available microstructure indicators for reduced pellets.

Finally, all the information can be expressed as the indicators' distribution from the 45,000 images composing a sample.

Table 3. Information available from the automated microscope for reduced pellets

Phase (% vol)	Sv of phase (cm^2/cm^3)	Sv of contact (cm^2/cm^3)	mls (µm)
Fe_{met}	Solids	Fe_{met} in contact with pore	Fe_{met}
Fe_{oxide}	Fe_{met}	Fe_{met} in contact with Fe_{oxide}	Fe_{oxide}
Porosity	Fe_{oxide}	Fe_{met} in contact with Fe_{met}	Porosity
	Porosity	Fe_{oxide} in contact with pore	
		Fe_{oxide} in contact with Fe_{oxide}	

The mass percentage of iron oxides and metallic iron can also be estimated based on the volume proportion of iron oxides and metallic iron and porosity given by the automated analysis, using densities of iron oxides (5.7 g/cm^3, assuming iron oxide as only FeO) and metallic iron (7.9 g/cm^3).

3. RESULTS AND DISCUSION

3.1 COREM R180 versus industrial DRI

Reduction behaviour of iron ore in the Midrex DR process was discussed in some publications [2, 3]. The evolution of the R180 reduction is closer to the evolution of industrial reduction than that of the DR90 [2, 3]. The microscopic examination of DRI produced in the R180 test and in a commercial plant showed [2] that the R180 test reproduces the physical structure and metallization characteristics of commercial DRI, as shown in Figure 1.

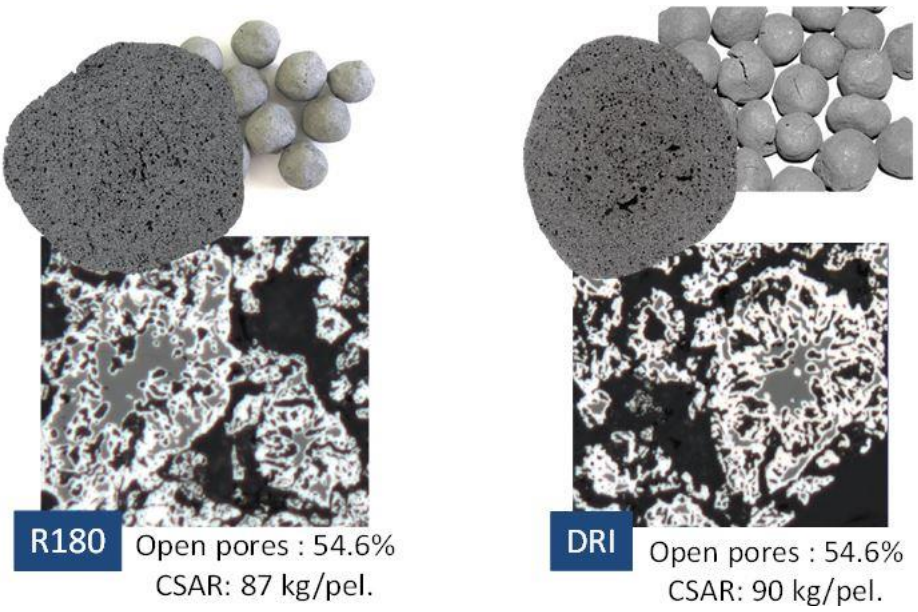

Figure 1. Comparison between industrial DRI and R180 DRI

3.2 COREM R180 versus ISO DR90

3.2.1 Final degree of reduction

Figure 2 presents the R180 and the DR90 data for various pellets (pot-grate and industrial samples). A similar range of final reduction was observed for both tests. However, a poor correlation can be observed between both tests.

Four arbitrary groups were created:

A. High R180 and low DR_{90}
B. High R180 and high DR_{90}
C. Low R180 and high DR_{90}
D. Low R180 and low DR_{90}

Samples from these groups were used in some of the following sub-sections and Figures.

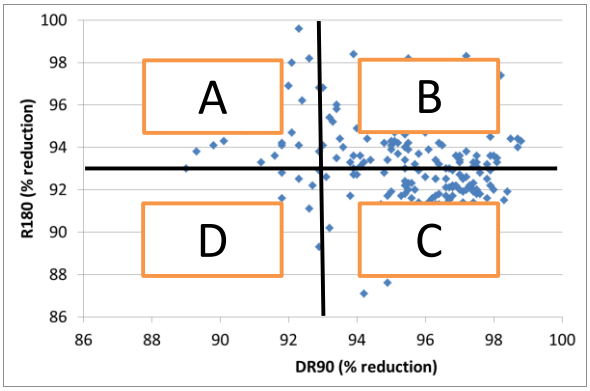

Figure 2. Comparison between the R180 and the DR90 results on various pellet samples

3.2.2 Reduction curves

Figure 3 presents two reduction curves for each of the four pellet groups and for both DR90 and R180 tests.

In Figure 3, it can be observed that the DR90 test classified pellets by reduction rate. However, it seems clear that the maximum reduction degree was not reached for almost all pellet samples tested under the DR90 conditions.

When looking at the R180 reduction curves in Figure 3, it can be observed that, at 90 min, the R180 test also classified pellets by reduction rate. Furthermore, it can be observed that, at 180 min, some pellet samples had reached a different maximum degree of reduction. Further in this paper, this will be referred to as “maximum achievable reduction degree”.

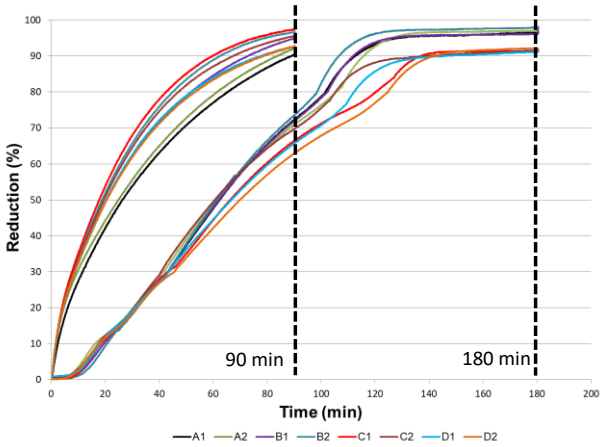

Figure 3. R180 and DR90 reduction curves of samples from the four pellet groups

3.2.3 Reduction steps

The DR90 test is an isothermal test using one gas composition for all the reduction duration, as described in Table 1. The thermodynamic equilibrium of Fe-O system with the gas is metallic iron.

The R180 test is a 3-stages non-isothermal test. It starts with a low temperature and a weaker reducing gas and moves towards higher temperatures and stronger reducing gas. The changes are based on the sample reduction evolution. More details can be found in reference [2]. One of the main differences between the R180 and the DR90 tests is that the thermodynamic equilibrium changes from magnetite to wustite to metallic iron in the R180 test.

3.2.4 Macrostructure evolution during reduction

This sub-section describes the macrostructure measured. Figure 4 shows the typical aspect of reduced pellets after final reduction under the R180 and the DR90 conditions.

It can be observed that pellets reduced under the DR90 test had more cracks than pellets reduced under the R180 test. The industrial DRI used as reference in this paper, as shown in Figure 1, was not cracked that much.

Figure 4. Typical aspect of reduced pellets after final reduction under the R180 and the DR90 conditions

Figure 5 presents the typical aspect of reduced pellets after a 10% and a 30% reduction under the R180 and the DR90 conditions. The DR90 test presented a more topochemical reduction pattern. It can be observed that, even at only 10% of reduction, metallic iron can be observed on the pellet's surface while there is still hematite in the core. On the opposite, the R180 reduction resulted in a more homogenous phase distribution in function of the pellet's radius.

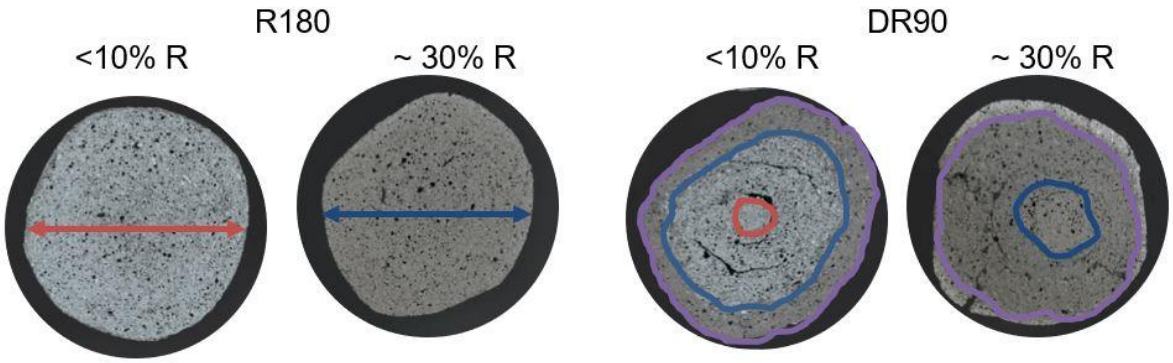

Figure 5. Typical aspect of reduced pellets after a 10% and a 30% reduction under the R180 and the DR90 conditions. Red: Hematite/magnetite; Blue: Magnetite/wustite; Purple: Wustite/metalic iron

3.3 Modified DR90 and R180

3.3.1 Initial reduction conditions versus final reduction

Figure 6 presents the R180 and the DR90 reduction curves for pellets D1. Furthermore, it also presents a longer DR90 test, extended to 180 min. The reduction time added to the DR90 test allowed to achieve a +4% reduction. This brought the reduction degree of the DR90 to 96.6%. It is also now more obvious that for pellet D1 reduced under DR90 conditions, 96.6% was the maximum achievable reduction degree.

Thus, a difference of 6% of the maximum achievable reduction degree can be observed between extended DR90 and R180 conditions (for sample D1).

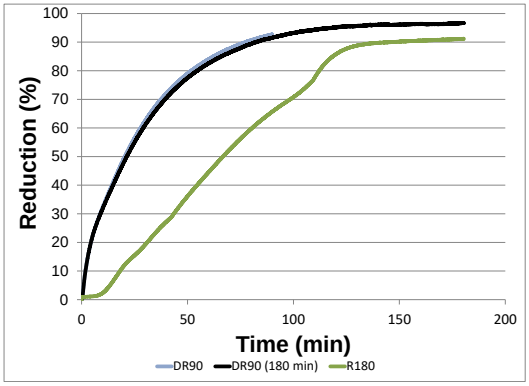

Figure 6. R180 and DR90 reduction curves for pellets D1

To understand which reducing conditions are responsible for the different maximum achievable reduction degree, four modified tests (Table 2) were performed. These four tests were also performed on pellet sample D1.

The first modified test reduced sample D1 up to 70%, using the DR90 conditions, and then up to 180 minutes, using the R180 conditions. Figure 7 presents the reduction curve of the modified tests on top of the regular DR90 and R180 tests as well as the extended DR90 tests. When comparing modification 1 with the non modifed tests, it can be observed, that the same maximum achievable reduction degree than the extended DR90 was achieved.

The second modified test reduced sample D1 up to 30%, using the DR90 conditions, and then up to 180 minutes, using the R180 conditions. Figure 7 shows that the same maximum achievable reduction degree than the extended DR90 was achieved. In both cases for modified tests 1 and 2, the initial reducing conditions resulted in the same maximum achievable reduction degree.

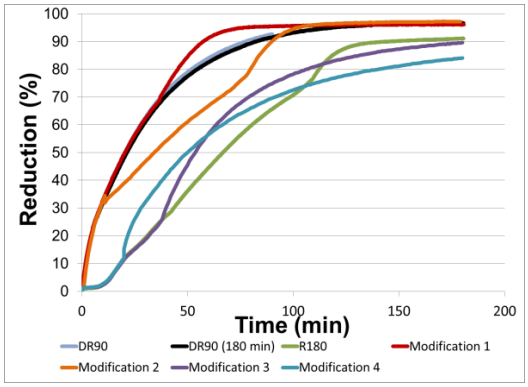

Figure 7. Modifications 1 to 4 (Table 2) reduction curves for pellets D1

The third modified test reduced the sample D1 up to 30%, using the R180 conditions, and then up to 180 minutes, using the DR90 conditions. Figure 7 shows that this time, the maximum achievable reduction degree achieved was the same as that of the R180 test. Therefore, once again in this third test, the initial reducing conditions resulted in a similar maximum achievable reduction degree.

The fourth and last modified test reduced sample D1 up to 10%, using R180 conditions, and then up to 180 minutes, using DR90 conditions. Figure 7 shows once again that the initial reducing conditions resulted in a similar maximum achievable reduction degree.

It seems that the difference in the maximum achievable reduction degree obtained with the R180 conditions or the extended DR90 condition is related to the initial conditions used for the reduction of hematite to magnetite and/or for the reduction of magnetite to wustite.

3.4 Evolution of microstructure during reduction

Numerous authors [4,5,6,7,8,9] have described the effects of temperature and reducing gas composition on microstructural changes of reduced products, mainly apparent volume and porosity. Temperature and gas composition of the DR90 and the R180 tests are different. Therefore, different microstructures of reduced products should be expected.

3.4.1 Magnetite formation

Porous magnetite was observed at the beginning of the reduction for both reduction tests. However, the magnetite generated during the DR90 test was more porous than the one generated during the R180 test (Figure 8).

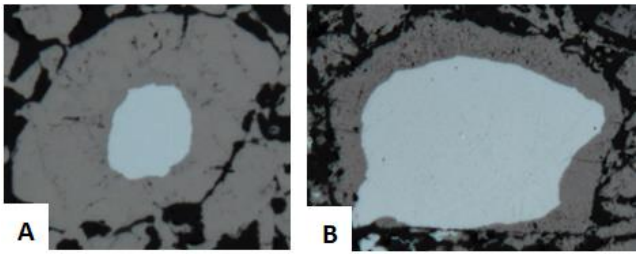

Figure 8. Magnetite generated during the R180 test (A) and the DR90 test (B) (brown: magnetite, white: hematite, black: porosity)

3.4.2 Wustite formation

Two types of wustite (dense and porous) were observed during both reduction tests. Most of the time, porous and dense wustite were observed inside the same particle. Once again, the porosity of wustite from the DR90 test was higher and predominant. The R180 test generated larger areas of dense wustite within particles when compared to the DR90 test, as shown in Figure 9.

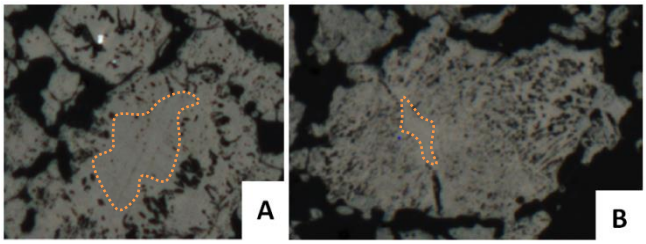

Figure 9. Wustite generated during the R180 (A) and the DR90 (B) tests

3.4.3 Metallic iron formation

It has been mentioned by some authors [10, 11] that only the porous iron morphology leads to a reasonable reaction time for reduction of wustite. This morphology allows direct gas access to the wustite surface.Dense iron layer prevents direct contact between gas and oxide and greatly affects the kinetics of the reduction.

Figure 10 shows the evolution of the metallic iron morphologies during the R180 and the DR90 tests. For both tests, iron nuclei formed within wustite particles and evolved to form metallic iron within porous wustite areas. In dense wustite areas or dense wustite particles, dense metallic iron surrounding dense wustite was observed. Obviously, the evolution of the metallic iron for both tests is more complex than this representation which describes the dominant mechanism. Areas of dense wustite surrounded by dense metallic iron in sample from the DR90 test were also observed, but mainly in a smaller size than in sample from R180 test.

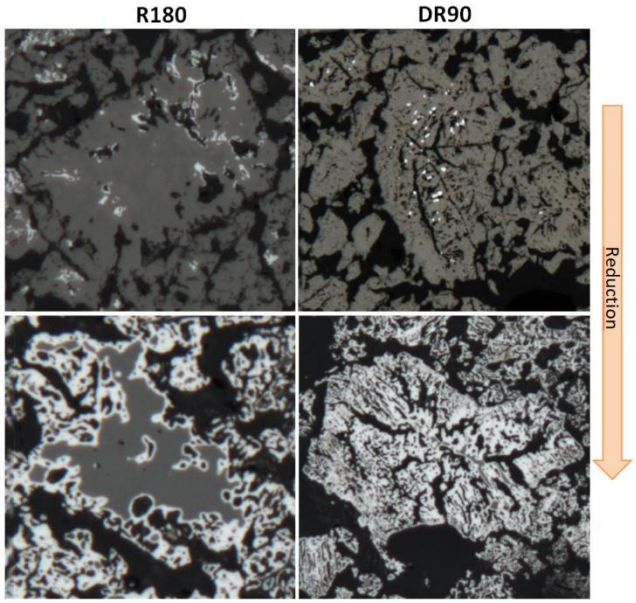

Figure 10. Metallic iron formation from the R180 and the DR90 tests
(white: metallic iron, grey: wustite, black: porosity)

3.4.4 Evolution of solids Sv

The data provided by the automated system were used in Figure 11 to show the evolution of the specific surface of solids during reduction for both tests.

It can be observed that the specific surface of solids increased during reduction due to the generation of porosity. This also meant that new gas-solid surfaces were generated during reduction.

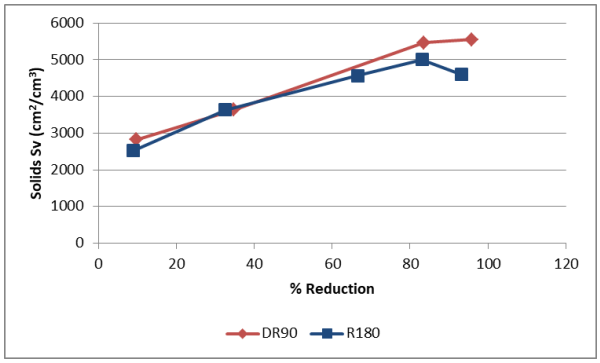

Figure 11. Evolution of Solids Sv in function of the reduction

It can also be observed in Figure 11 that the DR90 had a higher solids' specific surface at the end of reduction. When the solids' specific surface was used to calculate mls of solids, it can be observed that the particles at the end of the DR90 test were smaller than the particles at the end of the R180 test, as shown in Figure 12.

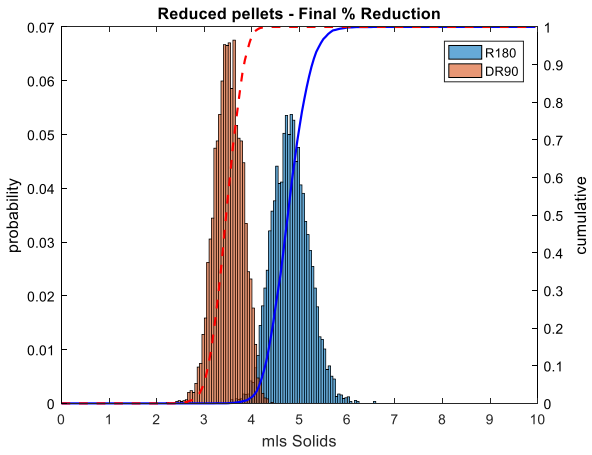

Figure 12. Distribution of solids mls (µm) at the end of the DR90 and the R180 tests

3.4.5 Evolution of Sv of pores in contact with Fe oxides

Figure 13 shows the evolution of the specific surface of pores in contact with an oxide surface during reduction. It can be observed that, as expected, this parameter decreased during the reduction.

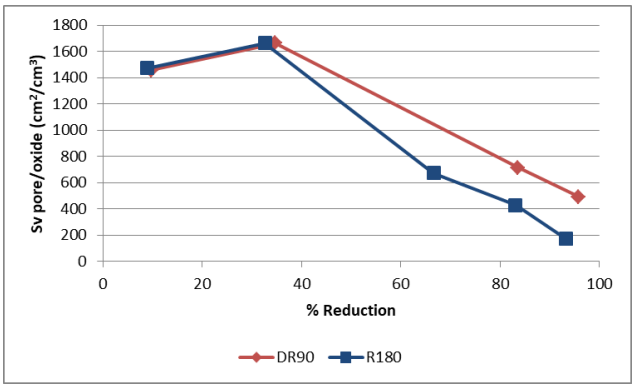

Figure 13. Specific surface of pores in contact with an oxide surface in function of reduction

The sample reduced under the R180 conditions had less oxide surface in contact with the reducing gas at the final reduction degree. Furthermore, Figure 14 shows that the mls of oxide particles after the R180 test were in average bigger than those of the DR90 test.

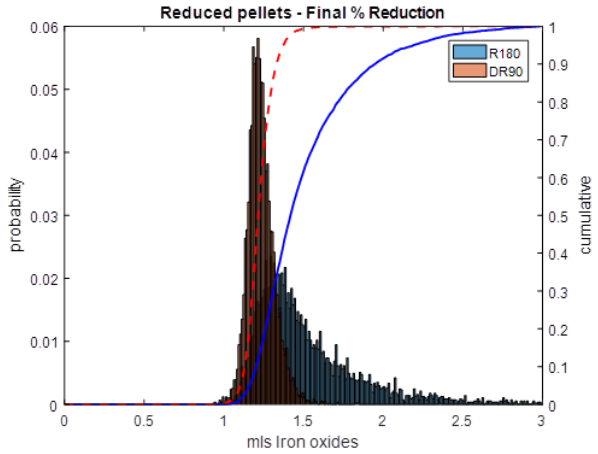

Figure 14. Distribution of oxides mls (µm) at the end of the DR90 and the R180 tests

4. CONCLUSION

Isothermal tests are simpler to perform and to reproduce between laboratories. They are designed to reproduce a phenomenon (swelling, clustering, desintegration, etc.). The COREM R180 better simulates the gas-based direct reduction process as it induces a pellet microstructure similar to commercial DRI. This is due to its non-isothermal conditions, which better represent gas-solids counter-current reactions occurring in industrial an DR shaft compared to an isothermal test.

The difference of maximum achievable reduction degree between the R180 and the DR90 tests was related to the beginning of the reduction. The microscopic observations showed that the morphologies of magnetite and wustite were different between both tests. The difference in dense wustite areas or dense wustite particles observed at the beginning of reduction likely explains the difference in dense metallic iron surrounding dense wustite areas at the final reduction degree. The slower diffusion within metallic iron layer, the lower final solids' specific surface and the

lower oxide surface in contact with the reducing gas were factors that could explain the lower maximum achievable reduction degree observed with the R180 conditions.

The paper also shows that mineralogical quantitative data from optical microscope can be useful to help guide R&D efforts in pellet development as well as pellet reduction.

REFERENCES

1 Lacroix O, Dubé M, Leclerc R, Laforest G, Firth, A. Relations between iron ore pellet induration reactions, microstructure and quality. In: Proceedings of the METEC & 2ndEstad 2015; 2015 June 15-19, Düsseldorf, Germany. p. 67-77.

2 Garant M, Ouellet G. Measurement of DR pellets reducibility. In: ISS 99; 1999.

3 Quatravaux T, Barros Lorenzo J, Maurice Y, Pierret H, Chen E, Tsvik G. Laboratory scale study of reduction kinetics of iron oxides on direct reduction conditions; In: Proceedings of the METEC & 2ndEstad 2015; 2015 June 15-19, Düsseldorf, Germany. p.557.

4 St.John D.H, Matthew S.P, Hayes P.C. Establishment of Product Morphology during the Initial Stages of Wustite Reduction. Metallurgical transactions B. 1984;15B:709.

5 St.John D.H, Matthew S.P, Hayes P.C. Breakdown of Dense Iron Layers on Wustite in CO/CO_2 and H_2/H_2O systems. Metallurgical transactions B. 1984;15B:701.

6 Matthew S.P, Cho T.R, Hayes P.C. Mechanism of Porous Iron Growth on Wustite and Magnetite during Gaseous Reduction. Metallurgical transactions B. 1990;21B:733.

7 Et-taribou M, Dupré B, Gleitzer C. Hematite Single Crystal Reduction into Magnetite with $CO-CO_2$. Metallugical transactions B. 1988;19B:311.

8 Husslage W.M, Bakker T, Kock M.E, Heerema R.H. Influence of reduction conditions on the expansion and microtexture of sintered hematite compacts during the transition to magnetite. Minerals & Metallurgical Processing. 1999; 16(3):23.

9 Brill-Edwards H, Daniell B.L, Samuel R.L, Shim F.I.M. Structural changes accompanying the reduction of polycrystalline hematite. Journal of the Iron and Steel Inst. 1965;203:361.

10 St.John D.H, Hayes P.C. Microstructural Features Produced by the Reduction of Wustite in H_2/H_2O Gas mixtures. Metallurgical transactions B. 1982;13B:117.

11 von Bogdandy L, Engell H.-J. The Reduction of Iron Ores, Springer-Verlag. Berlin Heidelber New York; 1971.